Two-dimensional Fröhlich interaction in transition-metal dichalcogenide monolayers: Theoretical modeling and first-principles calculations

Thibault Sohier,[1,2,*] Matteo Calandra,[1] and Francesco Mauri[3,4]

[1]*IMPMC, CNRS, Université Pierre et Marie Curie, 4 Place Jussieu, 75005 Paris, France*
[2]*Theory and Simulation of Materials (THEOS), École Polytechnique Fédérale de Lausanne, CH-1015 Lausanne, Switzerland*
[3]*Departimento di Fisica, Università di Roma La Sapienza, Piazzale Aldo Moro 5, I-00185 Roma, Italy*
[4]*Graphene Labs, Fondazione Istituto Italiano di Tecnologia, Via Morego, I-16163 Genova, Italy*

We perform *ab initio* calculations of the coupling between electrons and small-momentum polar-optical phonons in monolayer transition-metal dichalcogenides of the $2H$ type: MoS_2, $MoSe_2$, $MoTe_2$, WS_2, and WSe_2. The polar-optical coupling with longitudinal optical phonons, or Fröhlich interaction, is fundamentally affected by the dimensionality of the system. In a plane-wave framework with periodic boundary conditions, the Fröhlich interaction is affected by the spurious interaction between the two-dimensional (2D) material and its periodic images. To overcome this difficulty, we perform density functional perturbation theory calculations with a truncated Coulomb interaction in the direction perpendicular to the plane of the 2D material. We show that the two-dimensional Fröhlich interaction is much stronger than assumed in previous *ab initio* studies. We provide analytical models depending on the effective charges and dielectric properties of the materials to interpret our *ab initio* calculations. Screening is shown to play a fundamental role in the phonon-momentum dependency of the polar-optical coupling, with a crossover between two regimes depending on the dielectric properties of the material relative to its environment. The Fröhlich interaction is screened by the dielectric environment in the limit of small phonon momenta and sharply decreases due to stronger screening by the monolayer at finite momenta. The small-momentum regime of the *ab initio* Fröhlich interaction is reproduced by a simple analytical model, for which we provide the necessary parameters. At larger momenta, however, direct *ab initio* calculations of electron-phonon interactions are necessary to capture band-specific effects. We compute and compare the carrier relaxation times associated with the scattering by both LO and A_1 phonon modes. While both modes are capable of relaxing carriers on time scales under the picosecond at room temperature, their absolute importance and relative importance vary strongly depending on the material, the band, and the substrate.

I. INTRODUCTION

Among the rapidly expanding family of two-dimensional (2D) materials, monolayer transition-metal dichalcogenides (TMDs) offer particularly interesting features for electronic and optoelectronic applications [1–5]. Thanks to high carrier mobility and a direct band gap in the visible range, they can be included in 2D van der Waals heterostructures to fulfill various functionalities associated with light-matter interaction and electron transport. In this context, it is essential to reach a good understanding of carrier scattering [6–8], including the intrinsic contribution from the electron-phonon interaction. In TMDs and other polar materials, a peculiar coupling emerges between electrons and longitudinal optical (LO) phonons. Such polar phonons interact with electrons by inducing a polarization density. At small phonon momenta, this polar-optical coupling, or Fröhlich interaction, can become quite large compared to standard electron-phonon coupling (EPC). Dimensionality has an interestingly drastic effect on this interaction. Indeed, in the limit of zero phonon momentum, the Fröhlich interaction diverges in a material with three-dimensional (3D) periodicity, while it tends to a finite value in 2D materials. This effect can be traced back to the behavior of the long-range Coulomb interaction.

Density functional perturbation theory [9] (DFPT) is a powerful tool to simulate electron-phonon interactions. Associated with analytical models [10–12], this method can be used to establish quantitative models [13] of the Fröhlich interaction in bulk materials. Such a comprehensive and quantitative study of the Fröhlich interaction is still missing in the case of 2D materials. This is mainly due to the limitations of DFPT in the 2D framework. Indeed, DFPT relies on 3D periodic boundary conditions, implying the presence of periodic images when simulating low-dimensional systems. Since long-range Coulomb interactions between periodic images arise when low-dimensional systems are perturbed at small momenta [14], DFPT fails to account for the peculiarities of the Fröhlich interaction in 2D. In addition to those computational limitations, deriving analytical models of the Fröhlich interaction is not straightforward. In particular, the screening of the Coulomb interaction in 2D materials is a complex mechanism [15–19] requiring careful modeling.

In a previous *ab initio* study [20] of EPC in MoS_2, the small-momentum behavior of the 2D Fröhlich interaction was estimated by fitting a 2D analytical model on *ab initio* calculations. However, the calculations were performed at momenta too large to capture the effects of dimensionality and the analytical model only partially accounted for the complex screening occurring in 2D materials. The 2D Fröhlich interaction was found to participate only moderately to the coupling with optical phonons in MoS_2, with a small-momentum limit three times smaller than the value reported

---

*Corresponding author: thibault.sohier@epfl.ch

here. Consequently, it was often ignored in the following *ab initio* studies of EPC in TMDs [21,22]. As far as modeling of the interaction is concerned, a more sophisticated model [15–19] of screening in 2D materials was used to estimate the strength of the Fröhlich interaction in a recent work [23]. This was done in the case of an isotropic dielectric tensor for the monolayer and without the support of direct *ab initio* computation of electron-phonon interactions.

We recently implemented [24] the truncation of the Coulomb interaction between periodic images of 2D materials in the density functional theory (DFT) and DFPT package QUANTUM ESPRESSO [25] (QE). This technique enables us to isolate each slab and simulate electron-phonon interactions in a 2D framework. In this work we use this approach to compute the 2D Fröhlich interaction from first principles. We focus on the 2*H* polytypes of MoS$_2$, MoSe$_2$, MoTe$_2$, WS$_2$, and WSe$_2$. We propose developments on the analytical model of the Fröhlich interaction in 2D, especially concerning its screening in the case of a monolayer with anisotropic dielectric properties and for different dielectric environment on each side of the monolayer. We use *ab initio* calculations to estimate the parameters of this analytical model. The analytical model is used to interpret and support our calculations of the coupling to LO phonons, and a simple effective model is proposed to reproduce its small-momentum limit. The analytical model is also used to estimate the effect of the presence of a substrate on the Fröhlich interaction. Finally, we compute the inverse relaxation times associated with intraband scattering of carriers by LO and A_1 phonons. Large variations are observed from material to material. The relative importance of the LO and A_1 contributions strongly depends on the band in which we consider such scattering. In any case, optical phonons (LO and/or A_1) are shown to be capable of relaxing carriers on a time scale inferior to the picosecond at room temperature.

II. *AB INITIO* SIMULATIONS OF ELECTRON-PHONON COUPLING

We perform DFPT calculations of EPC in monolayer TMDs (2*H* type), using our recently developed 2D Coulomb cutoff approach [24] within the [25] QE distribution. This approach consists in truncating the Coulomb interaction between the periodic images of the 2D material. This was implemented for the computation of total energy, forces, phonons, and electron-phonon coupling. The technique requires the periodic images to be separated by at least twice the thickness of the electronic density of the simulated layer. We use a separation of ≈17 Å, largely fulfilling that requirement. Within a slab of thickness ≈12 Å, everything happens as if the monolayer was isolated. Further details about the implementation of the 2D Coulomb cutoff in the DFT and DFPT packages of the QE distribution method will be exposed in a separate publication. We use pseudopotentials from the Standard Solid-State Pseudopotentials (SSSP) library [26] (accuracy version) with Perdew-Burke-Ernzerhof functionals and kinetic energy cutoff as indicated in the library. Spin-orbit coupling is neglected. Starting from experimental lattice parameters [27], structures are relaxed to minimize the total energy in our DFT framework. The resulting in-plane lattice parameters a_0, subsequently used in our calculations, are given in Table IV.
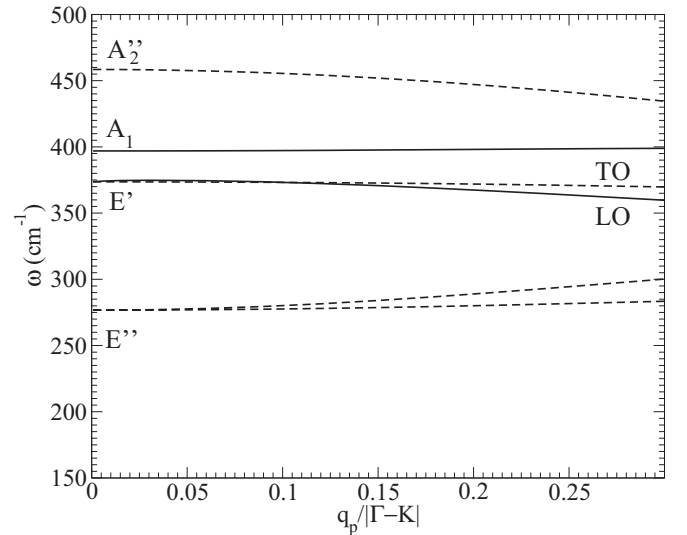

FIG. 1. Dispersion of the optical phonons in monolayer MoS$_2$ at small momenta. For the modes in dashed lines, EPC matrix elements are negligible. The A_1 and LO modes, in plain lines, couple to electrons. We follow the notation of Ref. [29] for the symmetry representations of the modes at Γ. The E' mode separates into LO and TO modes.

The electronic-momentum grid is set to $16 \times 16 \times 1$. Those choices are sufficient to obtain optical phonon energies within a few cm^{-1} of experimental values (when available).

In this section, MoS$_2$ is used as an example. We perform calculations in bulk MoS$_2$ as well to highlight the impact of dimensionality on the Fröhlich interaction. For bulk MoS$_2$, we use the standard QE distribution and the experimental [27] out-of-plane lattice parameter of $c = 12.29$ Å. The corresponding unit-cell includes two layers such that the interlayer distance in the bulk is ≈6.15 Å. Note that a rigorous study of the bulk requires the inclusion of dispersion corrections [28] to account for van der Waals interactions between layers. Since we only seek a comparison of the small-momentum behavior of the Fröhlich interaction, however, we ignore this aspect.

We note $\mathbf{e}_{\mathbf{q}_p \nu}$ and $\hbar\omega_{\mathbf{q}_p \nu}$ as the eigenvector and energy, respectively, associated with a phonon in branch ν with in-plane momentum $\mathbf{q}_p$. The dispersions of small-momentum optical phonons in MoS$_2$ are shown in Fig. 1. Among those, only the A_1 and LO modes (solid lines in Fig. 1) couple to electrons. In the small-momentum limit, the A_1 mode corresponds to out-of-plane displacements of the sulfur atoms in phase opposition, while the molybdenum atoms are static. The LO mode corresponds to in-plane longitudinal displacements with the molybdenum atom moving in phase opposition to both sulfur atoms. A more extensive *ab initio* study of phonons in MoS$_2$ and WS$_2$ can be found in Ref. [29]. Optical phonon modes at small momenta are qualitatively similar for all the TMDs studied in this work.

We consider phonon-scattering of an electron from state $|\mathbf{k}\rangle$ to $|\mathbf{k} + \mathbf{q}\rangle$ within a given band. The associated EPC matrix element is defined as

$$g_\nu(\mathbf{q}_p) = \sum_{a,i} \sqrt{\frac{\hbar}{2 M_a \omega_{\mathbf{q},\nu}}} \mathbf{e}_{\mathbf{q}_p,\nu}^{a,i} \langle \mathbf{k} + \mathbf{q} | \Delta_{\mathbf{q}_p}^{a,i} \mathcal{V}_{KS}(\mathbf{r}) | \mathbf{k} \rangle, \quad (1)$$
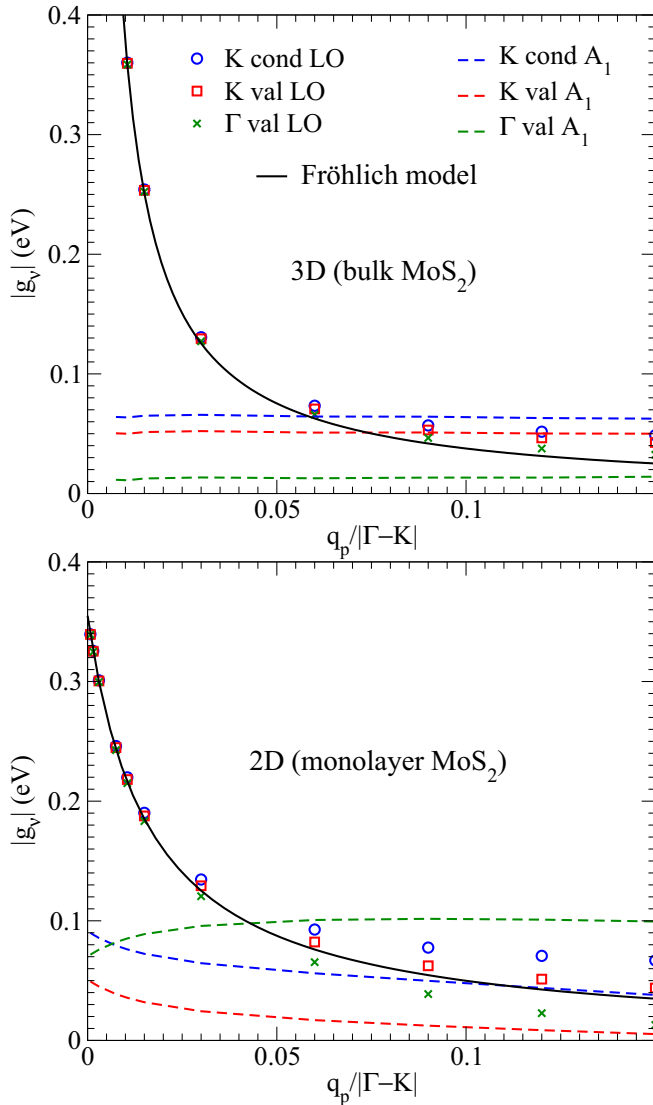
FIG. 2. EPC matrix elements involving LO and A_1 phonon modes in bulk and monolayer MoS_2. We consider intraband scattering of electrons or holes in the conduction band near **K** ("K cond") and in the valence band near **K** and Γ ("K val" and "Γ val," respectively). Momenta $\mathbf{q}_p$ are in the $\Gamma \to \mathbf{M}$ direction. The coupling to the LO phonons includes the Fröhlich interaction. The models for three-dimensional and two-dimensional Fröhlich interactions in bulk and monolayer MoS2 are represented in solid lines and described in the text. Dashed lines and symbols are DFPT calculations. The standard QE package was used for the bulk, while we used our implementation of the Coulomb cutoff in for the monolayer.

where M_a is the mass of atom a and $\Delta_{\mathbf{q}_p}^{a,i} \mathcal{V}_{KS}(\mathbf{r})$ is the lattice periodic part of the derivative of the self-consistent Kohn-Sham potential with respect to a phonon displacement of atom a in direction i.

We consider neutral TMDs to avoid the metallic nature of the electronic screening that would occur in doped layers. Our primary goal is the study of the long-range Fröhlich interaction, involving LO phonons at small momenta ($|\mathbf{q}_p| < 15\%$ of $|\Gamma - \mathbf{K}|$) and an excited electron or hole. Considering the small-momenta restriction and the energy of LO phonons, we can focus on intraband scattering. We further narrow

the study to the highest part of the valence band around the high-symmetry points **K** and Γ, and the lowest part of the conduction band around **K**. More precisely, we compute the EPC matrix elements $g_{LO}(\mathbf{q}_p)$ for the following pairs of electronic states: (i) $\mathbf{k} = \mathbf{K} - \mathbf{q}_p/2$ and $\mathbf{k} + \mathbf{q}_p = \mathbf{K} + \mathbf{q}_p/2$ in the conduction band, noted "K cond"; (ii) $\mathbf{k} = \mathbf{K} - \mathbf{q}_p/2$ and $\mathbf{k} + \mathbf{q}_p = \mathbf{K} + \mathbf{q}_p/2$ in the valence band, noted "K val"; (iii) $\mathbf{k} = \Gamma - \mathbf{q}_p/2$ and $\mathbf{k} + \mathbf{q}_p = \Gamma + \mathbf{q}_p/2$ in the valence band, noted "Γ val." Momentum $\mathbf{q}_p$ is in the $\Gamma \to \mathbf{M}$ direction to minimize LO/TO mixing.

The results of the calculations for MoS_2 are presented in Fig. 2. For comparison, we add the coupling $g_{A_1}(\mathbf{q}_p)$ associated with the other significant contribution of the A_1 mode. We recover the characteristic behaviors of the 2D and 3D Fröhlich interactions. In the 3D case, the interaction diverges as $\mathbf{q}_p \to \Gamma$. In the 2D framework provided by our approach, however, the Fröhlich interaction tends to a constant at Γ. Note that a divergence will occur when using the standard QE code, even if the interlayer distance is increased. The fact that we recover the finite limit of the coupling at Γ thus confirms that the truncation of the Coulomb interaction in QE is equivalent to simulating an isolated monolayer. The coupling to LO phonons at large momenta depends on the bands via the details of the electronic wave functions. Indeed, in that case, the variations of the polarization potential on the length scale of the width of the electronic states become relevant. Similar calculations were performed for monolayers of $MoSe_2$, $MoTe_2$, WS_2, and WSe_2; see Fig. 8 in Appendix B.

In Figs. 2 and 8, the solid lines represent analytical models discussed in the following sections. In those models, we focus on the more general small-momentum behavior of the Fröhlich interaction, which depends solely on the Born effective charges and dielectric properties of the material. From a modeling point of view, the existence of finite limit at Γ for the 2D interaction is easily established by considering the $1/|\mathbf{q}_p|$ dependence of the 2D Coulomb interaction in reciprocal space. The sharp decreasing of the coupling at finite-q, however, is a more subtle screening effect that remains to be studied in detail. Our numerical DFPT method provides us with a support to treat this issue in a systematic manner and establish a quantitatively accurate analytical model.

III. ANALYTICAL MODELS OF THE FRÖHLICH INTERACTION

We now present analytical models to explain our DFPT calculations and gain better understanding of the effect of dimensionality on the small-momentum limit of the Fröhlich interaction. The tensors of Born effective charges are noted $\mathcal{Z}_a^b$ and $\mathcal{Z}_a^m$ for bulk and monolayer, respectively. The index a runs over the atoms of the unit cell. The relative dielectric permittivity tensors (simply called dielectric tensors hereafter) for bulk and monolayer are noted $\mathcal{E}^b$ and $\mathcal{E}^m$, respectively. By symmetry, the tensors are isotropic in the plane, but we allow for different properties in the out-of-plane direction. The tensors thus have the following generic forms:

$$\mathcal{E} = \begin{pmatrix} \epsilon_p & 0 & 0 \\ 0 & \epsilon_p & 0 \\ 0 & 0 & \epsilon_z \end{pmatrix} \quad \mathcal{Z}_a = \begin{pmatrix} Z_{a,p} & 0 & 0 \\ 0 & Z_{a,p} & 0 \\ 0 & 0 & Z_{a,z} \end{pmatrix}. \quad (2)$$

In-plane and out-of-plane variables are separated according to the notation $\mathbf{r} \to (\mathbf{r}_p, z)$ and $\mathbf{q} \to (\mathbf{q}_p, q_z)$. We use Gaussian centimeter-gram-second (CGS) units.

A. Three-dimensional bulk

We quickly recall the well-known results of the 3D case. The small-momentum behavior of the Fröhlich interaction is well described by the leading order in Vogl's model [10]

$$\left| g_{\text{Fr}}^{\text{3D}}(\mathbf{q}_p) \right| = \frac{4\pi e^2}{V|\mathbf{q}_p|\epsilon_p^b} \sum_a \frac{\mathbf{e}_{\mathbf{q}_p} \cdot \mathcal{Z}_a^b \cdot \mathbf{e}_{\mathbf{q}_p\text{LO}}^a}{\sqrt{2M_a\omega_{\mathbf{q}_p\text{LO}}}}, \quad (3)$$

where e is the elementary charge, V is the unit cell's volume, ϵ_p^b is the in-plane dielectric constant of the bulk (15.37 in MoS_2), and $\mathbf{e}_{\mathbf{q}_p} = \mathbf{q}_p/|\mathbf{q}_p|$. The prefactor of $1/|\mathbf{q}_p|$ is essentially constant in the range of momenta considered in this work. A small dependency on norm and direction of $\mathbf{q}_p$ appears as the phonon modes deviate from the strictly longitudinal modes. This model is sufficient to reproduce the small-momentum limit of the Fröhlich interaction, as shown in Fig. 2, where the plain line is the above model.

B. Two-dimensional monolayer

Our objective is to derive the Fröhlich interaction in the system of Fig. 3. We consider LO phonons in a 2D material of thickness t. Its dielectric tensor $\mathcal{E}^m$ has the form of Eq. (2), with in-plane and out-of-plane dielectric constants ϵ_p^m and ϵ_z^m, respectively. Above and below are two semi-infinite spaces with isotropic dielectric properties represented by the dielectric constants ϵ_2 and ϵ_1, respectively.

The origin of the polar-optical coupling is the polarization density $\mathbf{P}(\mathbf{r}_p, z)$ generated by the atomic displacement pattern associated with a LO phonon of in-plane momentum $\mathbf{q}_p$,

$$\mathbf{P}(\mathbf{r}_p, z) = \frac{e^2}{A} \sum_a \frac{\mathcal{Z}_a^m \cdot \mathbf{e}_{\mathbf{q}_p\text{LO}}^a}{\sqrt{2M_a\omega_{\mathbf{q}_p\text{LO}}}} f(z) e^{i\mathbf{q}_p \cdot \mathbf{r}_p}, \quad (4)$$
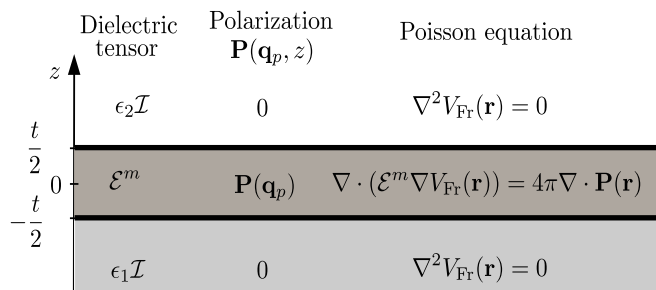

FIG. 3. Model of the Fröhlich interaction in a polar 2D material of thickness t. LO phonons generate a periodic polarization density $\mathbf{P}(\mathbf{r}_p, z) = \mathbf{P}(\mathbf{q}_p, z)e^{i\mathbf{q}_p \cdot \mathbf{r}_p}$ inside the 2D material. The dielectric properties of the 2D material are represented by the dielectric tensor $\mathcal{E}^m$ with in-plane and out-of-plane dielectric constants ϵ_p^m and ϵ_z^m, respectively. Above and below are two half spaces in which the polarization is zero and the dielectric constants are ϵ_2 and ϵ_1, respectively. The symbol $\mathcal{I}$ denotes the identity matrix. The two thick horizontal black lines represent surface charges at the interfaces of the 2D material due to the abrupt variations in the polarization density. We write the Poisson equation defining the Fröhlich potential V_{Fr} in each region.

where A is the area of the unit cell and $f(z)$ is the out-of-plane profile of the polarization (normalized to unity). Such a polarization density induces a potential $V_{\text{Fr}}(\mathbf{r}_p, z) = V_{\text{Fr}}(\mathbf{q}_p, z)e^{i\mathbf{q}_p \cdot \mathbf{r}_p}$ with the same periodicity. The associated EPC can then be written as

$$g_{\text{Fr}}^{\text{2D}}(\mathbf{q}_p) = \int V_{\text{Fr}}(\mathbf{q}_p, z)n_{el}(z)dz, \quad (5)$$

where $n_{el}(z)$ is the plane-averaged electronic density. By using this expression, we neglect the details of the wave functions and the associated band dependency. In the out-of-plane direction, we consider the electronic density and the polarization to be uniform over the thickness t of the material

$$f(z) = n_{el}(z) = \frac{\theta(t/2 - |z|)}{t}, \quad (6)$$

where θ is the Heaviside function. This approximation should be satisfactory in the long-wavelength limit, since $V_{\text{Fr}}(\mathbf{q}_p, z)$ varies mildly in the out-of-plane direction.

The potential V_{Fr} must fulfill the Poisson equation

$$\nabla \cdot [\mathcal{E}(z)\nabla V_{\text{Fr}}(\mathbf{r})] = 4\pi\nabla \cdot \mathbf{P}(\mathbf{r}), \quad (7)$$

where $\mathcal{E}(z)$ is a position-dependent dielectric tensor. The central objects of the problem are the phonon-induced polarization density and the dielectric tensor. As one travels along the out-of-plane direction, both those quantities change. Inside the 2D material, $\mathcal{E}(z) = \mathcal{E}^m$ and the polarization density is finite and oscillating in the plane. Outside the 2D material, $\mathcal{E}(z) = \epsilon_1\mathcal{I}$ or $\epsilon_2\mathcal{I}$ (where $\mathcal{I}$ is the identity matrix) and the polarization density is zero. Other requirements on the potential are that that the associated in-plane electric field $\mathbf{E}^{\parallel}(\mathbf{r})$ and out-of-plane electric displacement $\mathbf{D}^{\perp}(\mathbf{r})$ should be continuous.

The detailed derivation of the solution to this model can be found in Appendix A. To allow for a more direct interpretation of the final solution in Eq. (A22), we seek a more transparent form. By Taylor expansion of the denominator at the linear order in $|\mathbf{q}_p|$, the full expression of Eq. (A22) can be recast in the form

$$\left| g_{\text{Fr}}^{\text{2D}}(\mathbf{q}_p) \right| = \frac{C_{\mathcal{Z}}}{\epsilon_{\text{eff}}(|\mathbf{q}_p|)},$$

$$\epsilon_{\text{eff}}(|\mathbf{q}_p|) \approx \epsilon_{\text{eff}}^0 + r_{\text{eff}}|\mathbf{q}_p|, \quad (8)$$

where the expressions of the parameters are given in Table I. The above form is found to reproduce Eq. (A22) very accurately. Only when $\epsilon_z^m \approx \epsilon_1$ or ϵ_2 should one retain Eq. (A22) rather than use Eq. (8). More quantitative results, depending on the nature of the monolayer, will be given in Sec. V. For now, let us make some qualitative remarks valid as long as the material is a stronger dielectric as the environment, which is the case of the monolayer TMDs discussed in this work, in vacuum or on SiO_2. The bare magnitude of the polar-optical coupling is given by $C_{\mathcal{Z}}$. The origin of the sharp decrease at finite $\mathbf{q}_p$ is a screening effect specific to 2D materials. It can be associated with the formation of surface charges due to the change in dielectric properties at the interfaces between the 2D material and its environment. The screening is characterized by the parameter r_{eff} which depends on the dielectric properties of the material as well as its thickness. Homogeneous to a distance,

TABLE I. Full expressions of the parameters involved in the model of the 2D Fröhlich interaction, Eq. (8). See Fig. 3 and Eq. (2) for the definitions of the various parameters in the model. Note that for the isolated TMDs considered in our *ab initio* calculations, we have $\epsilon_1 = \epsilon_2 = \epsilon_{12} = 1$, $\epsilon_z^m \gg 1$, and $\epsilon_p^m \gg 1$, which leads to $F \approx 1$, $\epsilon_{\text{eff}}^0 \approx 1$, and $r_{\text{eff}} \approx \frac{\epsilon_p^m t}{2}$.

$$C_{\mathcal{Z}} = \frac{2\pi e^2}{A} \sum_a \frac{\mathbf{e}_{\mathbf{q}_p} \cdot \mathcal{Z}_a^m \cdot \mathbf{e}_{\mathbf{q}_p\text{LO}}^a}{\sqrt{2 M_a \omega_{\mathbf{q}_p\text{LO}}}}$$

$$\epsilon_{\text{eff}}^0 = \epsilon_{12} \frac{\epsilon_z^m \bar{\epsilon}}{\epsilon_z^m \bar{\epsilon} + \epsilon_{12}(\epsilon_p^m - \bar{\epsilon})}$$

$$r_{\text{eff}} = \frac{(\epsilon_{\text{eff}}^0)^2}{\epsilon_{12}} \left(\frac{\epsilon_{12}}{3\epsilon_z^m} + \frac{\epsilon_p^m}{2\epsilon_{12}} F \right) \times t$$

$$F = 1 + \frac{\epsilon_1 \epsilon_2}{\bar{\epsilon}^2} + \frac{\epsilon_{12}}{\bar{\epsilon}} - \frac{\epsilon_{12}^2}{\bar{\epsilon}\epsilon_z^m} - \frac{\epsilon_{12}^2}{\bar{\epsilon}^2} - \frac{\epsilon_{12}}{\epsilon_z^m}$$

$$\epsilon_{12} = \frac{\epsilon_1 + \epsilon_2}{2}, \bar{\epsilon} = \sqrt{\epsilon_z^m \epsilon_p^m}$$

it can be interpreted as an effective thickness marking the crossover between two screening regimes. For $|\mathbf{q}_p| \ll r_{\text{eff}}^{-1} \epsilon_{\text{eff}}^0$, the coupling is screened by ϵ_{eff}^0, which depends mainly on the dielectric properties of the environment. For $|\mathbf{q}_p| \gg r_{\text{eff}}^{-1} \epsilon_{\text{eff}}^0$, the field lines are confined to the material, and the coupling is screened by the material. Materials with large dielectric constants (with respect to the environment) will tend to focus the field lines more strongly, which results in a larger effective thickness r_{eff} and a sharper decrease in the Fröhlich interaction at finite momenta (note that the slope of the coupling at Γ is proportional to $-r_{\text{eff}}$).

We have derived the general expression for an anisotropic slab and different dielectric media above and below. It can be applied to any polar material. To be quantitatively predictive, we need to evaluate the parameters involved. We now detail how to evaluate those parameters with *ab initio* calculations.

IV. *AB INITIO* PARAMETERS

Here again, MoS$_2$ will be used as an example to illustrate the method. The final parameters of interest will then be given for the other TMDs. The parameters of the model are the Born effective charges, dielectric tensors, and phonon eigenvectors. The dynamical matrix and the corresponding phonon eigenvectors are available from the electron-phonon calculations. The QE code computes clamped-ion dielectric tensors and Born effective charges by means of linear response calculations with respect to an electric field perturbation [9]. The Born effective charges are related to the derivative of the forces on the atoms with respect to the applied electric field. Since our implementation of the 2D Coulomb cutoff includes the computation of forces, the Born effective charges can be computed in the 2D framework for the monolayers. Note, however, that equivalent results can be obtained with the standard code. Indeed, Born effective charges converge relatively fast towards their 2D values with respect to the distance between periodic images. The dielectric constant, on the other hand, is computed as a macroscopic quantity defined over a three-dimensional supercell. As such, the computation

TABLE II. Dielectric constants and effective charges of bulk and monolayer MoS$_2$ as obtained in DFT. In the case of the monolayer, we report the dielectric constant in the case of an isotropic model. The full range of possible values for the in-plane and out-of-plane dielectric constants is given in Fig. 5.

Bulk		Monolayer	
Symbol	Value	Symbol	Value
ϵ_p^b	15.37	$\epsilon_p^m = \epsilon_{\text{iso}}^m$	15.5
ϵ_z^b	6.57	$\epsilon_z^m = \epsilon_{\text{iso}}^m$	15.5
$Z_{\text{Mo},p}^b$	−0.9413	$Z_{\text{Mo},p}^m$	−1.0051
$Z_{\text{Mo},z}^b$	−0.5918	$Z_{\text{Mo},z}^m$	−0.0919
$Z_{\text{S},p}^b$	0.4668	$Z_{\text{S},p}^m$	0.4525
$Z_{\text{S},z}^b$	0.2921	$Z_{\text{S},z}^m$	0.0411

of the dielectric tensor of the bulk $\mathcal{E}^b$ is straightforward and reported in Table II for MoS2. The computation of an equivalent quantity relevant for 2D materials, however, raises issues beyond periodic images interactions [30,31]. As of yet, we did not implement the modifications necessary to compute dielectric tensors in a 2D framework. In the following, the dielectric tensors of the monolayers will be evaluated using the standard QE code, with an effort to extract relevant 2D quantities from 3D calculations.

The constant $C_{\mathcal{Z}}$ corresponds to the magnitude of the *bare* Fröhlich interaction. It depends on the Born effective charges and the phonon displacements. The components of the tensors $\mathcal{Z}_a^m$ (computed with 2D Coulomb cutoff) and $\mathcal{Z}_a^b$ (computed without cutoff) for MoS$_2$ are given in Table II. The components of $\mathcal{Z}_a^m$ for other monolayer TMDs are reported in Table III. The bare coupling $C_{\mathcal{Z}}$ varies with the direction and modulus of $\mathbf{q}_p$ via the phonon eigenvectors. It reaches a maximum in the $\mathbf{q}_p \rightarrow \Gamma$ limit, where the LO eigenvectors correspond to purely longitudinal modes. It moderately decreases with increasing momenta ($\approx -10\%$ at $|\mathbf{q}_p| \approx 15\%$ of $|\Gamma - \mathbf{K}|$). Since the momentum behavior of the Fröhlich interaction is largely dominated by the screening factor $\frac{1}{\epsilon_{\text{eff}}(\mathbf{q}_p)}$, we can neglect the variations associated with the phonon eigenvectors and use the $\mathbf{q}_p \rightarrow \Gamma$ value of the bare coupling. Those values are reported in Table IV, in the column labeled "$C_{\mathcal{Z}}$ (*ab initio*)."

We now evaluate the dielectric properties of the monolayer using the standard (3D) QE code. We simulate a system made of repeated monolayers separated by a varying distance c, with vacuum in between. The clamped-ion dielectric tensor of this

TABLE III. Effective charges of monolayer TMDs, as computed in QE via the response to an external electric field. $M \equiv$ Mo, W; $X \equiv$ S, Se, Te.

Monolayer	$Z_{M,p}^m$	$Z_{M,z}^m$	$Z_{X,p}^m$	$Z_{X,z}^m$
MoS$_2$	−1.00	−0.09	0.45	0.04
MoSe$_2$	−1.78	−0.13	0.73	0.04
MoTe$_2$	−3.14	−0.15	1.36	0.04
WS$_2$	−0.49	−0.07	0.20	0.02
WSe$_2$	−1.17	−0.12	0.43	0.03

TABLE IV. Comparison of relevant quantities involved in the Fröhlich interaction for the monolayer TMDs MoS_2, $MoSe_2$, $MoTe_2$, WS_2, and WSe_2. a_0 is the lattice parameter. We report here the dielectric constants associated with the simplest isotropic model, that is, $\epsilon_{iso}^m = \epsilon_p^m = \epsilon_z^m$ and $t = t_{iso}$. Note that we use the fact that $r_{eff} \approx \epsilon_{iso}^m t_{iso}/2$. For the bare Fröhlich interaction C_Z, we report both the fitted value (from fit) used in the plots to reproduce the DFPT data and the value found by computing effective charges and phonons eigenvectors (*ab initio*).

Monolayer	a_0(Å)	t_{iso} (Å)	ϵ_{iso}^m	r_{eff} (Å)	C_Z (eV) (from fit)	C_Z (eV) (*ab initio*)	ω_{LO} (cm^{-1})	ω_{A_1} (cm^{-1})
MoS_2	3.18	6.00	15.5	46.5	0.355	0.334	373.7	396.9
$MoSe_2$	3.32	5.94	17.9	53.2	0.521	0.502	277.5	235.4
$MoTe_2$	3.56	6.65	20.9	69.5	0.819	0.819	223.6	162.9
WS_2	3.18	5.52	15.2	42.0	0.165	0.140	345.9	407.4
WSe_2	3.31	5.97	16.3	48.7	0.323	0.276	239.4	242.1

system, as computed within QE, is written as

$$\mathcal{E}^{QE} = \begin{pmatrix} \epsilon_p^{QE} & 0 & 0 \\ 0 & \epsilon_p^{QE} & 0 \\ 0 & 0 & \epsilon_z^{QE} \end{pmatrix}. \qquad (9)$$

In this picture, the dielectric tensor of the bulk simply corresponds to $\mathcal{E}^{QE}$ with a fixed interlayer distance c (neglecting the small effects of an alternating stacking). To relate $\mathcal{E}^{QE}$ to the dielectric tensor of the monolayer $\mathcal{E}^m$, we use effective medium theory and introduce the thickness of the monolayer as a parameter. We then have the following relations [32]:

$$\epsilon_p^{QE} = 1 + (\epsilon_p^m - 1)t/c,$$

$$\frac{1}{\epsilon_z^{QE}} = 1 - \frac{(\epsilon_z^m - 1)}{\epsilon_z^m} t/c. \qquad (10)$$

Note that in the limit of infinite interlayer distance, this dielectric tensor does not tend toward $\mathcal{E}^m$. Instead, it tends towards the dielectric tensor of vacuum.

In Fig. 4, we plot the ϵ_p^{QE} and $1/\epsilon_z^{QE}$ as functions of $1/c$. Fitting this data, we find slopes $s_1 = 87.2$ Å and $s_2 = 5.62$ Å, respectively. We then write ϵ_p^m and ϵ_z^m as functions of t according to

$$\epsilon_p^m = 1 + \frac{s_1}{t},$$
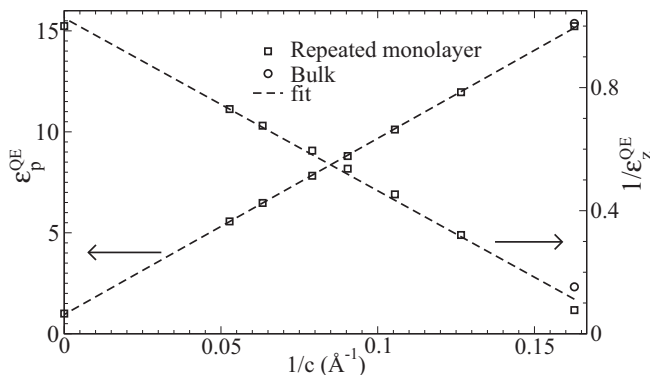
$$\epsilon_z^m = \frac{t}{t - s_2}. \qquad (11)$$

FIG. 4. The QE quantities ϵ_p^{QE} and $1/\epsilon_z^{QE}$ as functions of the inverse interlayer distance $1/c$, in MoS_2. In each plot, we add the data point corresponding to the bulk.

In principle, every set of values $\{\epsilon_p^m, \epsilon_z^m, t\}$ that satisfies the above equations can fit our DFT results. We can assume that $t > s_2$, as we would have $\epsilon_z^m < 0$ otherwise. We can also assume that $t < c_{bulk} \approx 6.15$ Å, the distance between two monolayers in the bulk. In Fig. 5, we plot $\epsilon_p^m, \epsilon_z^m$ as functions of t in this reasonable range of values for the thickness. Figure 5 should thus be understood as a set of possible values for $\epsilon_p^m, \epsilon_z^m$ and the corresponding thickness. Note that $t \approx 6$ Å is consistent with the width of the equilibrium electronic density found in DFT. One can see that while ϵ_p^m is almost constant in Fig. 5, the variation of ϵ_z^m is more pronounced. Similar results are obtained for $MoSe_2$, $MoTe_2$, WS_2, and WSe_2. As far as the above *ab initio* study is concerned, we are thus left with a free parameter to model the dielectric properties of the 2D materials, that is, a choice to make for the set of values $\{\epsilon_p^m, \epsilon_z^m, t\}$. For all TMDs, there is a reasonable value of $t = t_{iso}$ leading to an isotropic model with $\epsilon_{iso}^m = \epsilon_p^m = \epsilon_z^m$. As shown in the next section, this isotropic model is a choice that leads to simple yet accurate results for the Fröhlich interaction.

V. EFFECTIVE ISOTROPIC MODEL

We now establish a simple effective model to reproduce the small-momentum limit of our direct DFPT calculations of the coupling to LO phonons. We first discuss the effects of selecting different set of values for ϵ_p^m, ϵ_z^m, and t. This depends on the dielectric environment, namely on the average dielectric constant $\epsilon_{12} = \frac{\epsilon_1 + \epsilon_2}{2}$. Our DFPT calculations are performed in vacuum, with $\epsilon_{12} = 1$. Whatever thickness we choose in
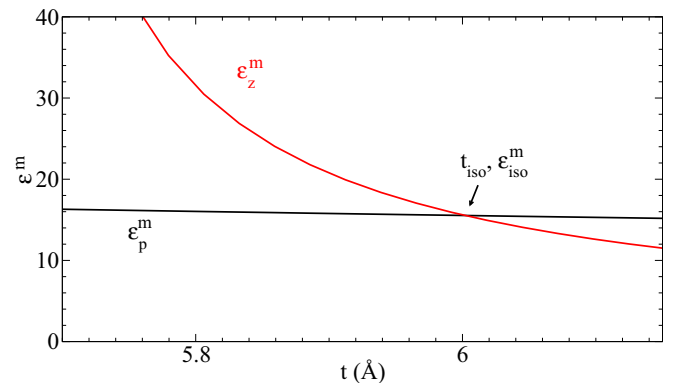

FIG. 5. Values of ϵ_p^m and ϵ_z^m that would be consistent with direct *ab initio* computation of the supercell's dielectric constants ϵ_p^{QE} and ϵ_z^{QE}, as functions of the corresponding thickness of the monolayer. We indicate the point corresponding to an isotropic system.
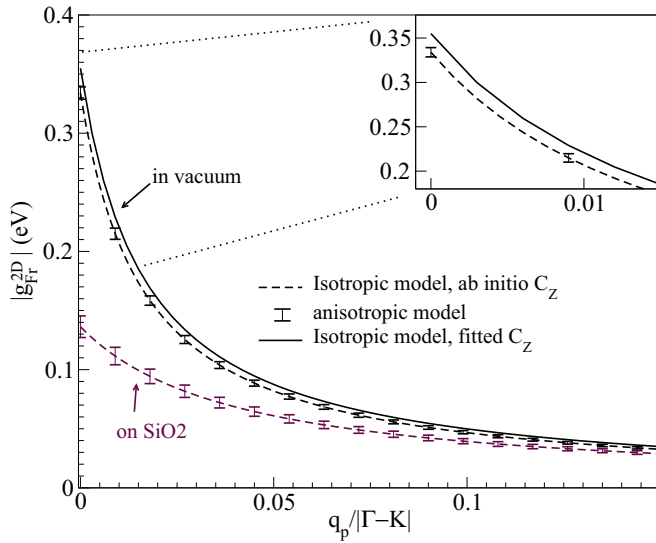
FIG. 6. Dashed lines are obtained by using the isotropic model ($\epsilon_{\mathrm{iso}}^m = \epsilon_p^m = \epsilon_z^m$, $t = t_{\mathrm{iso}}$) and $C_{\mathcal{Z}}$ from *ab initio* Born effective charges. The errors bars show the deviation from the isotropic model obtained by using an anisotropic model with values of ϵ_p^m, ϵ_z^m, and t in the range of Fig. 5. The solid line corresponds to the isotropic model (for MoS$_2$ in vacuum) with fitted $C_{\mathcal{Z}}$. This coincides with the direct DFPT calculations of EPC, at least at small momenta (see Figs. 2 and 8). The inset is a magnification on the small momenta limit of the models. It shows that a fitted $C_{\mathcal{Z}}$ is necessary, as an anisotropic model would not be enough to fit the direct DFPT calculations of EPC. The SiO$_2$ substrate increases the screening of the Fröhlich interaction strongly at small momenta.

Fig. 5, we have $\epsilon_p^m \gg \epsilon_{12}$ and $\epsilon_z^m \gg \epsilon_{12}$. In that case, the anisotropic model is very close to the isotropic one. This is shown numerically in Fig. 6. The isotropic model, for which we use $\epsilon_{\mathrm{iso}}^m = \epsilon_p^m = \epsilon_z^m$ and $t = t_{\mathrm{iso}}$, is shown as dashed lines. The error bars represent the deviation of the full anisotropic model when using other values of ϵ_p^m, ϵ_z^m, and t within those represented in Fig. 5.

For most monolayers, using the bare Fröhlich interaction $C_{\mathcal{Z}}$ calculated via the *ab initio* effective charges leads to a slight mismatch with respect the direct DFPT calculations of EPC. The effect of anisotropy in vacuum is too small to explain this mismatch, as seen in Fig. 6. To reach better agreement, the parameter $C_{\mathcal{Z}}$ must be adjusted. The fitted values of $C_{\mathcal{Z}}$ for all monolayers are reported in Table IV. Note that *ab initio* and fitted values stay relatively close, meaning that a simple calculation of the effective charges can still lead to a good approximation of the bare Fröhlich interaction. However, the mismatch is clear enough to point to some possible issues in the computation of the effective charges. This imprecision on the computation of $C_{\mathcal{Z}}$ also implies that we cannot resolve the very small effect of anisotropy.

Overall, an isotropic model with dielectric constant $\epsilon_{\mathrm{iso}}^m = \epsilon_p^m = \epsilon_z^m$ and a fitted $C_{\mathcal{Z}}$ (solid lines in Figs. 2 and 8 of Appendix B) is the best choice to reproduce our DFPT results. Within the assumption that $\epsilon_{\mathrm{iso}}^m \gg \epsilon_{12}$, further simplification and greater clarity can be achieved in the model. Indeed, the

parameters of Table I can be approximated by

$$\epsilon_{\mathrm{eff}}^0 \approx \epsilon_{12} = \frac{\epsilon_1 + \epsilon_2}{2}, \qquad (12)$$

$$r_{\mathrm{eff}} \approx \frac{\epsilon_{\mathrm{iso}}^m}{2} t_{\mathrm{iso}}. \qquad (13)$$

This simple form allows us to gain physical insight on the screening. In the limit $r_{\mathrm{eff}}|\mathbf{q}_p| \gg \epsilon_{12}$, that is, $|\mathbf{q}_p| \gg \frac{2\epsilon_{12}}{\epsilon_{\mathrm{iso}}^m t_{\mathrm{iso}}}$, we have $g_{\mathrm{Fr}}^{2D}(|\mathbf{q}_p|) \approx g_{\mathrm{Fr}}^{3D}(|\mathbf{q}_p|)$. Indeed, the factor $1/2$ in r_{eff} makes it possible to recover the prefactor of the 3D Coulomb interaction ($2\pi e^2 \rightarrow 4\pi e^2$), while $At \approx V$, and $\epsilon_{\mathrm{iso}}^m = \epsilon_p^m \approx \epsilon_p^b$. In that case, the wavelength of the perturbation associated with the LO phonon is small and the associated field lines stay inside the monolayer. The interaction is then screened by the monolayer. In the $r_{\mathrm{eff}}|\mathbf{q}_p| \ll \epsilon_{12}$ limit, that is, $|\mathbf{q}_p| \ll \frac{2\epsilon_{12}}{\epsilon_{\mathrm{iso}}^m t_{\mathrm{iso}}}$, we have $g_{\mathrm{Fr}}^{2D}(|\mathbf{q}_p|) \approx \frac{C_{\mathcal{Z}}}{\epsilon_{12}}$, which corresponds to the interaction being screened solely by the environment. In vacuum, the crossover between those two regimes happens for $|\mathbf{q}_p|$ around $\frac{2}{\epsilon_{\mathrm{iso}}^m t_{\mathrm{iso}}} \approx 0.02\,\text{\AA}^{-1} \approx 0.015|\Gamma - \mathbf{K}|$, that is, very close to the Γ point. This is due to the large dielectric constant of the monolayer compared to the environment.

An important benefit of the model is the possibility to evaluate the effects of the dielectric environment [33]. In Fig. 6, we present results for the more experimentally relevant case of MoS$_2$ ion SiO$_2$, for which $\epsilon_{12} = \frac{1+3.9}{2} = 2.45$. The coupling is shown to be strongly decreased overall. The validity of the approximations $\epsilon_p^m \gg \epsilon_{12}$ and $\epsilon_z^m \gg \epsilon_{12}$ is less clear, and the deviation from the isotropic model in Fig. 5 is more discernible. However, for the purpose of estimating the effect of a SiO$_2$ substrate, and, given the simplicity of the above parameters, it is still convenient to use the effective isotropic model.

The relevant parameters, including the thickness t_{iso} and isotropic dielectric constant $\epsilon_{\mathrm{iso}}^m$, are reported in Table IV for all monolayers. In the case of MoS$_2$, we find that the value of the coupling at Γ in vacuum, i.e., the bare interaction $C_{\mathcal{Z}}$, is three times larger than the one predicted in a previous *ab initio* study [20]. The bare interaction $C_{\mathcal{Z}}$ and effective screening length r_{eff} increase with the atomic number of the chalcogen while they decrease with the atomic number of the transition metal.

VI. TRANSPORT

To provide a more practical sense of the implications of this work, we compute the following inverse relaxation times for an excited electron or hole scattered by LO or A_1 phonons

$$\frac{1}{\tau_\nu(\varepsilon_{\mathbf{k}})} = \frac{2\pi}{\hbar} \sum_{\mathbf{q}_p} |g_\nu(\mathbf{q}_p)|^2$$

$$\times \delta\big(\varepsilon_{\mathbf{k}+\mathbf{q}_p} - \varepsilon_{\mathbf{k}} \mp \hbar\omega_{\mathbf{q}_p,\nu}\big) \begin{Bmatrix} N_{\nu,\mathbf{q}_p} \\ N_{\nu,\mathbf{q}_p} + 1 \end{Bmatrix}, \qquad (14)$$

where $\nu \equiv$ LO or A_1, $N_{\nu,\mathbf{q}_p}$ is the Bose-Einstein distribution for phonon occupation at room temperature, and $\varepsilon_{\mathbf{k}}$ is the eigenvalue energy of electronic state $|\mathbf{k}\rangle$, measured from the bottom (top) of the conduction (valence) band. The "$-$" (respectively "$+$") sign in the Dirac δ function δ is associated with $N_{\nu,\mathbf{q}_p}$ ($N_{\nu,\mathbf{q}_p} + 1$) and corresponds to phonon absorption (emission). The two contributions are then summed. In Fig. 7,
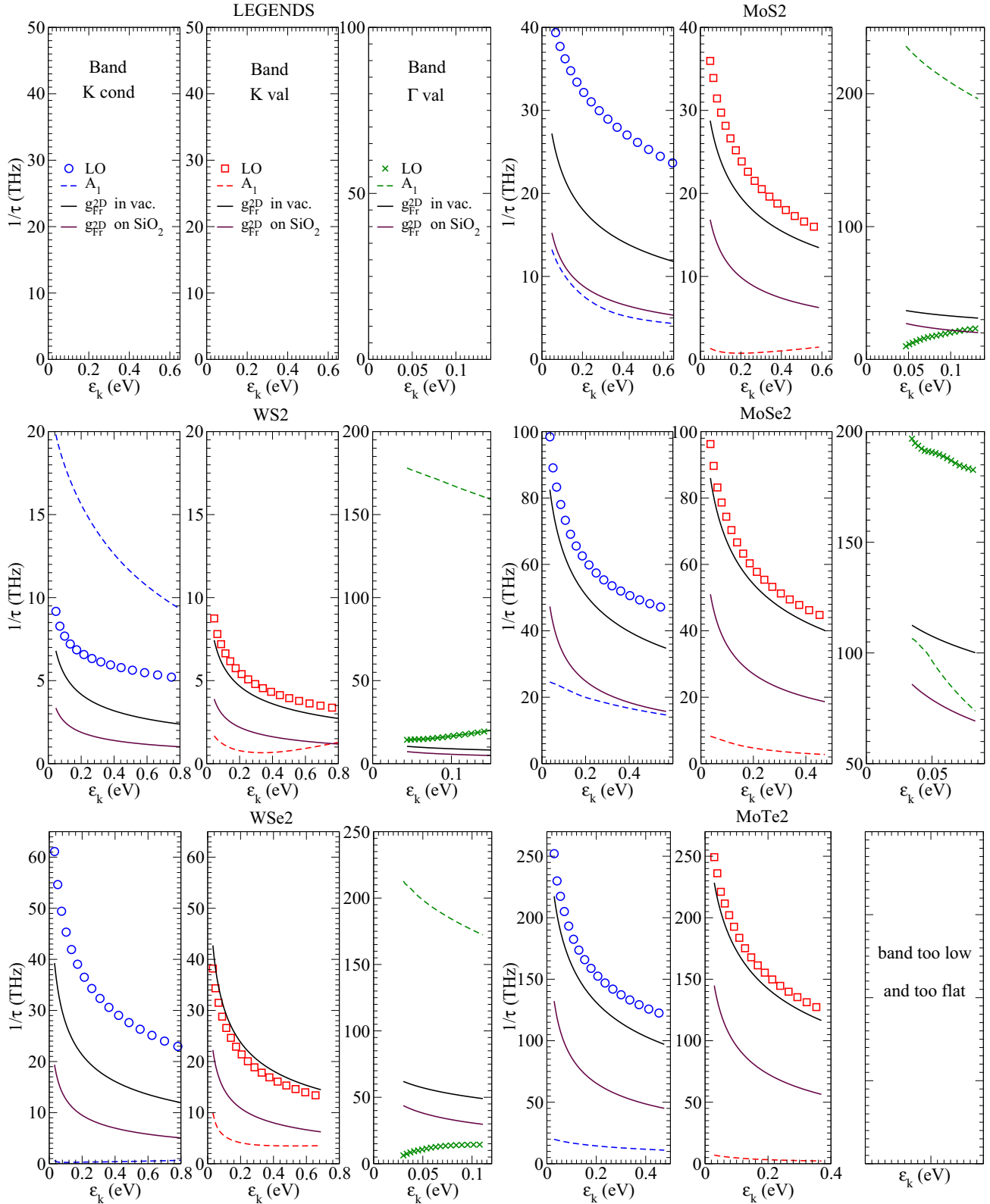
FIG. 7. Inverse relaxation times associated with the scattering by LO mode, A_1 mode, and the Fröhlich models for monolayer MoS_2, $MoSe_2$, $MoTe_2$, WS_2, and WSe_2. Calculations were performed at room temperature. In the case of the valence band around the Γ point of $MoTe_2$, the effective mass is so large that the norm of the phonon wave vectors $|\mathbf{q}_p|$ involved in the scattering processes go beyond the scope of this work. In any case, this band is far below the valence band at $\mathbf{K}$, such that it would not be involved in transport.

TABLE V. Effective masses are estimated using the results of Ref. [34].

Monolayer	m^*/m_0 K cond	m^*/m_0 K val	m^*/m_0 Γ val
MoS_2	0.45	0.57	2.52
$MoSe_2$	0.54	0.65	3.70
$MoTe_2$	0.56	0.72	20.0
WS_2	0.31	0.42	2.17
WSe_2	0.34	0.45	2.79

we plot the inverse relaxation times for each of the three bands (K cond, K val, and Γ val) and for each of the MoS_2, $MoSe_2$, $MoTe_2$, WS_2, and WSe_2 monolayers. To compute those quantities, we need EPC matrix elements on a fine grid of momenta $\mathbf{q}_p$. We use the analytical model when possible and linearly extrapolate the DFPT couplings otherwise. More precisely, in the limit of small momenta, the coupling to LO phonons follows our analytical model of the Fröhlich interaction and does not depend on the angle of momentum $\mathbf{q}_p$ or the band. We then use the analytical model $|g_{Fr}^{2D}(\mathbf{q}_p)|$. At larger momenta, the coupling depends on the band via the wave functions. We then extrapolate the *ab initio* coupling $|g_{LO}(\mathbf{q}_p)|$. A few other *ab initio* calculations were performed for momenta up to $|\mathbf{q}_p^{max}| \approx 0.3|\Gamma - \mathbf{K}|$. A mild angular dependency is possible for the *ab initio* matrix elements $|g_{LO}(\mathbf{q}_p)|$ and $|g_{A_1}(\mathbf{q}_p)|$. We neglect this angular dependency. The integral of Eq. (14) depends on the coupling and the effective masses of the corresponding band. We use effective masses from Ref. [34], reported in Table V. We probe electronic states with electronic momenta $|\mathbf{k}| < |\mathbf{q}_p^{max}|/2$. This implies that the range of carrier energies we consider depends on the effective masses. Note that only for MoS_2 is it clear that the valence band at Γ should be considered. For the others, this band is lower in energy. For more information about the band structures of these materials; see Ref. [28].

Figure 7 shows that optical phonons are capable of relaxing excited carriers on a time scale inferior to the picosecond at room temperature. The strength of the Fröhlich interaction depends on the material considered, mainly via the variations of Born effective charges. However, this is far from being the only aspect to account for when studying relaxation times. Figure 7 shows a great disparity of the results depending on the phonon mode, the band, and the material. The analytical model of the Fröhlich interaction is a good estimate of the DFPT calculations only for the valence band at $\mathbf{K}$. The relaxation times depend strongly on the band-specific, large-momentum values of the coupling with LO phonons. This is due to the fact that at the minimum carrier energy ($\varepsilon_\mathbf{k} = \hbar\omega_{LO}$), the integral of Eq. (14) already involves relatively large phonon momenta $|\mathbf{q}_p|$. The strength of the coupling with A_1 phonons and thus the relative importance of the scattering by LO and A_1 phonons also depends strongly on the bands. Very few comments apply globally. LO phonons seem to dominate optical-phonon scattering around $\mathbf{K}$, for all monolayers except WS_2. A_1 phonons seem to dominate in the valence band around Γ for all monolayers except $MoSe_2$. Although the analytical model with *ab initio* parameters is useful for suspended samples in the small-momentum limit to interpret the phenomenon, interpolate the coupling or to estimate the

effect of the dielectric environment, direct DFPT calculations of EPC for each band is essential. The great disparity in the relaxation times and the number of phenomenon affecting it highlight the need for direct *ab initio* simulations of electron-phonon interactions in a two-dimensional framework. Furthermore, some additional effects should be included for a quantitative comparison with experiment. This work is a study of the coupling with optical phonons at small momenta and should provide useful guidelines to interpret experimental transport data. However, in a full quantitative study of transport properties, one need to account for spin-orbit coupling, doping effects, the scattering of electrons in the Q band, the scattering between different bands. Those issues can be treated in the framework of QE with 2D Coulomb cutoff.

VII. CONCLUSION

We have implemented the truncation of the Coulomb interaction in the plane-wave and phonon codes of the QUANTUM ESPRESSO package. This method enables us to simulate the small-momentum limit of the Fröhlich interaction in a 2D framework, for monolayer TMDs MoS_2, $MoSe_2$, $MoTe_2$, WS_2, and WSe_2. We show that this limit is three times larger than previously assumed in the case of MoS_2 in vacuum. We develop analytical models for the Fröhlich interaction in 2D materials, along with *ab initio* methods to evaluate the parameters involved. A simple isotropic model is found to reproduce the small-momentum limit of our DFPT calculations. We provide the parameters of this model for the various TMDs studied. We show that screening is paramount to evaluate the strength of the Fröhlich interaction. In particular, the dielectric environment of the 2D material has a strong influence on the small-momentum limit of the interaction. Namely, the interaction is reduced by a factor $\frac{\epsilon_1 + \epsilon_2}{2}$ with respect to vacuum, where ϵ_1 and ϵ_2 are the dielectric constant of the environment on each side the monolayer. We consider intraband scattering within the valence and conduction bands around $\mathbf{K}$ and within the valence band around Γ. Above a certain value of the momentum ($\approx 10\%$ of $|\Gamma - \mathbf{K}|$), the band-dependent form of the electronic wave functions plays a role in the Fröhlich interaction and DFPT calculations are necessary to evaluate deviations from the analytical model. Finally, we evaluate the inverse relaxation times associated with the scattering of photoexcited carriers by LO and A_1 phonons. Those modes are shown to be capable of relaxing carriers on time scales smaller than the picosecond. The efficiency of carrier relaxation by optical phonons in TMDs is found to depend on many parameters. In addition to the strength of the Fröhlich interaction depending on the monolayer, the large momentum, band-specific coupling affects the relaxation times. Depending on the material and the band, the relaxation time associated with the A_1 mode can also be quite large. It is not correct to neglect scattering by either LO or A_1 phonons globally. Overall, the complexity and disparity highlighted in this work points to the necessity of relying on direct *ab initio* calculations of electron-phonon interactions in a 2D framework.

APPENDIX A: ANALYTICAL MODEL OF THE 2D FRÖHLICH INTERACTION

We solve here the model described in the main text, Sec. III B. The dielectric properties of the system are

$$\mathcal{E}(z) = \begin{cases} \epsilon_1 \mathcal{I} & \text{if } z < -t/2, \\ \mathcal{E}^m & \text{if } z < |t/2|, \\ \epsilon_2 \mathcal{I} & \text{if } z > t/2. \end{cases} \quad \text{(A1)}$$

The potential V_{Fr} must solve the Poisson equation:

$$\nabla \cdot [\mathcal{E}^m \nabla V_{\text{Fr}}(\mathbf{r}_p, z)] = 4\pi \nabla \cdot \mathbf{P}(\mathbf{r}_p, z) \quad \text{if } |z| < t/2,$$

$$\nabla^2 V_{\text{Fr}}(\mathbf{r}_p, z) = 0 \qquad \text{if } |z| > t/2. \quad \text{(A2)}$$

The associated parallel electric field and orthogonal electric displacement,

$$\mathbf{E}^{\|}(\mathbf{r}_p, z) = -\frac{\partial V_{\text{Fr}}(\mathbf{r}_p, z)}{\partial \mathbf{r}_p}, \quad \text{(A3)}$$

$$\mathbf{D}^{\perp}(\mathbf{r}_p, z) = \begin{cases} -\epsilon_1 \frac{\partial V_{\text{Fr}}(\mathbf{r}_p, z)}{\partial z} & \text{if } z < -t/2, \\ -\epsilon_z^m \frac{\partial V_{\text{Fr}}(\mathbf{r}_p, z)}{\partial z} & \text{if } |z| < t/2, \\ -\epsilon_2 \frac{\partial V_{\text{Fr}}(\mathbf{r}_p, z)}{\partial z} & \text{if } z > t/2, \end{cases} \quad \text{(A4)}$$

must be continuous.

The general solution to the differential equation of Eq. (A2) is the sum of the solution to the homogeneous equation and a particular solution:

$$V_{\text{Fr}}(\mathbf{q}_p, z) = V_h(\mathbf{q}_p, z) + V_p(\mathbf{q}_p, z). \quad \text{(A5)}$$

The homogeneous equation is

$$\nabla \cdot [\mathcal{E}^m \nabla V_h(\mathbf{r}_p, z)] = 0 \quad \text{if } |z| < t/2,$$

$$\nabla^2 V_h(\mathbf{r}_p, z) = 0 \quad \text{if } |z| > t/2, \quad \text{(A6)}$$

and the particular solution solves Eq. (A2). To find a particular solution, we first solve Eq. (A2) inside the anisotropic material,

$$\nabla \cdot [\mathcal{E}^m \nabla V_p(\mathbf{r})] = 4\pi e^2 \frac{i|\mathbf{q}_p|}{A} \quad \text{(A7)}$$

$$\times \sum_a \frac{\mathbf{e}_{\mathbf{q}_p} \cdot \mathcal{Z}_a^m \cdot \mathbf{e}_{\mathbf{q}_p \text{LO}}^a}{\sqrt{2M_a \omega_{\mathbf{q}_p \text{LO}}}} f(z) e^{i\mathbf{q}_p \cdot \mathbf{r}_p}, \quad \text{(A8)}$$

$$V_p(\mathbf{q}_p, q_z) = \frac{-2i C_{\mathcal{Z}} |\mathbf{q}_p|}{\epsilon_p^m |\mathbf{q}_p|^2 + \epsilon_z^m q_z^2} f(q_z), \quad \text{(A9)}$$

$$V_p(\mathbf{q}_p, z) = \frac{-i C_{\mathcal{Z}}}{\sqrt{\epsilon_p^m \epsilon_z^m}} \int_{-\infty}^{+\infty} e^{-\tilde{\mathbf{q}}_p |z' - z|} f(z') dz', \quad \text{(A10)}$$

with $\tilde{\mathbf{q}}_p = \sqrt{\frac{\epsilon_p^m}{\epsilon_z^m}} \mathbf{q}$, and $C_{\mathcal{Z}}$ is defined in Table I. Using $f(z') = \frac{\theta(t/2 - |z'|)}{t}$, we get for $z \in [-t/2; t/2]$

$$V_p(\mathbf{q}_p, z) = \frac{-i C_{\mathcal{Z}}}{\sqrt{\epsilon_p^m \epsilon_z^m}} \frac{2}{|\tilde{\mathbf{q}}_p| t} [1 - e^{-|\tilde{\mathbf{q}}_p| t/2} \cosh(|\tilde{\mathbf{q}}_p| z)], \quad \text{(A11)}$$

where cosh is the hyperbolic cosine function. We need to extend this particular solution outside the material. We do not require the particular solution to carry any physical meaning outside the material. It only needs to fulfill

$$\nabla^2 V_p(\mathbf{r}_p, z) = 0 \quad \text{if } |z| > t/2. \quad \text{(A12)}$$

We simply choose the solution of the above equation such that the corresponding out-of-plane electric field is continuous at the interfaces. This solution exists, and since we only need its values at the interfaces, it is not necessary to specify it further.

Let us proceed to the homogeneous solution. Knowing that $V_h(\mathbf{r}) = V_h(\mathbf{q}_p, z) e^{i\mathbf{q}_p \cdot \mathbf{r}_p}$, the homogeneous equation Eq. (A6) reduces to

$$\frac{\partial^2 V_h(\mathbf{q}_p, z)}{\partial z^2} = \frac{\epsilon_p^m}{\epsilon_z^m} |\mathbf{q}_p|^2 V_h(\mathbf{q}_p, z) \quad \text{if } |z| < t/2,$$

$$\frac{\partial^2 V_h(\mathbf{q}_p, z)}{\partial z^2} = |\mathbf{q}_p|^2 V_h(\mathbf{q}_p, z) \qquad \text{if } |z| > t/2. \quad \text{(A13)}$$

Adding the condition that the potential must vanish for $|z| \to \infty$, the solution to the homogeneous equation, Eq. (A6), has the form

$$V_h(\mathbf{q}_p, z) = \begin{cases} c_3 e^{-|\mathbf{q}_p| z} & \text{if } z > t/2, \\ c_1 e^{|\tilde{\mathbf{q}}_p| z} + c_2 e^{-|\tilde{\mathbf{q}}_p| z} & \text{if } |z| < t/2, \\ c_4 e^{|\mathbf{q}_p| z} & \text{if } z < -t/2, \end{cases} \quad \text{(A14)}$$

with $\tilde{\mathbf{q}}_p = \sqrt{\frac{\epsilon_p^m}{\epsilon_z^m}} \mathbf{q}$. Note that the homogeneous solution has the form of a potential generated by two surface charges at the interfaces of the monolayer. The continuity of the potential gives

$$c_3 e^{-|\mathbf{q}_p| t/2} = c_1 e^{|\tilde{\mathbf{q}}_p| t/2} + c_2 e^{-|\tilde{\mathbf{q}}_p| t/2}, \quad \text{(A15)}$$

$$c_4 e^{-|\mathbf{q}_p| t/2} = c_1 e^{-|\tilde{\mathbf{q}}_p| t/2} + c_2 e^{|\tilde{\mathbf{q}}_p| t/2}. \quad \text{(A16)}$$

The continuity of the parallel electric field is fulfilled by construction. We use the continuity of the out-of-plane electric displacement Eq. (A4) to obtain

$$\frac{C_{\mathcal{Z}}}{\sqrt{\epsilon_p^m \epsilon_z^m}} (\epsilon_z^m - \epsilon_1) \frac{1 - e^{-|\tilde{\mathbf{q}}_p| t}}{|\mathbf{q}_p| t} = (\epsilon_1 + \sqrt{\epsilon_p^m \epsilon_z^m}) c_1 e^{|\tilde{\mathbf{q}}_p| t/2}$$

$$+ (\epsilon_1 - \sqrt{\epsilon_p^m \epsilon_z^m}) c_2 e^{-|\tilde{\mathbf{q}}_p| t/2},$$

$$\frac{C_{\mathcal{Z}}}{\sqrt{\epsilon_p^m \epsilon_z^m}} (\epsilon_z^m - \epsilon_2) \frac{1 - e^{-|\tilde{\mathbf{q}}_p| t}}{|\mathbf{q}_p| t} = (\epsilon_2 - \sqrt{\epsilon_p^m \epsilon_z^m}) c_1 e^{-|\tilde{\mathbf{q}}_p| t/2}$$

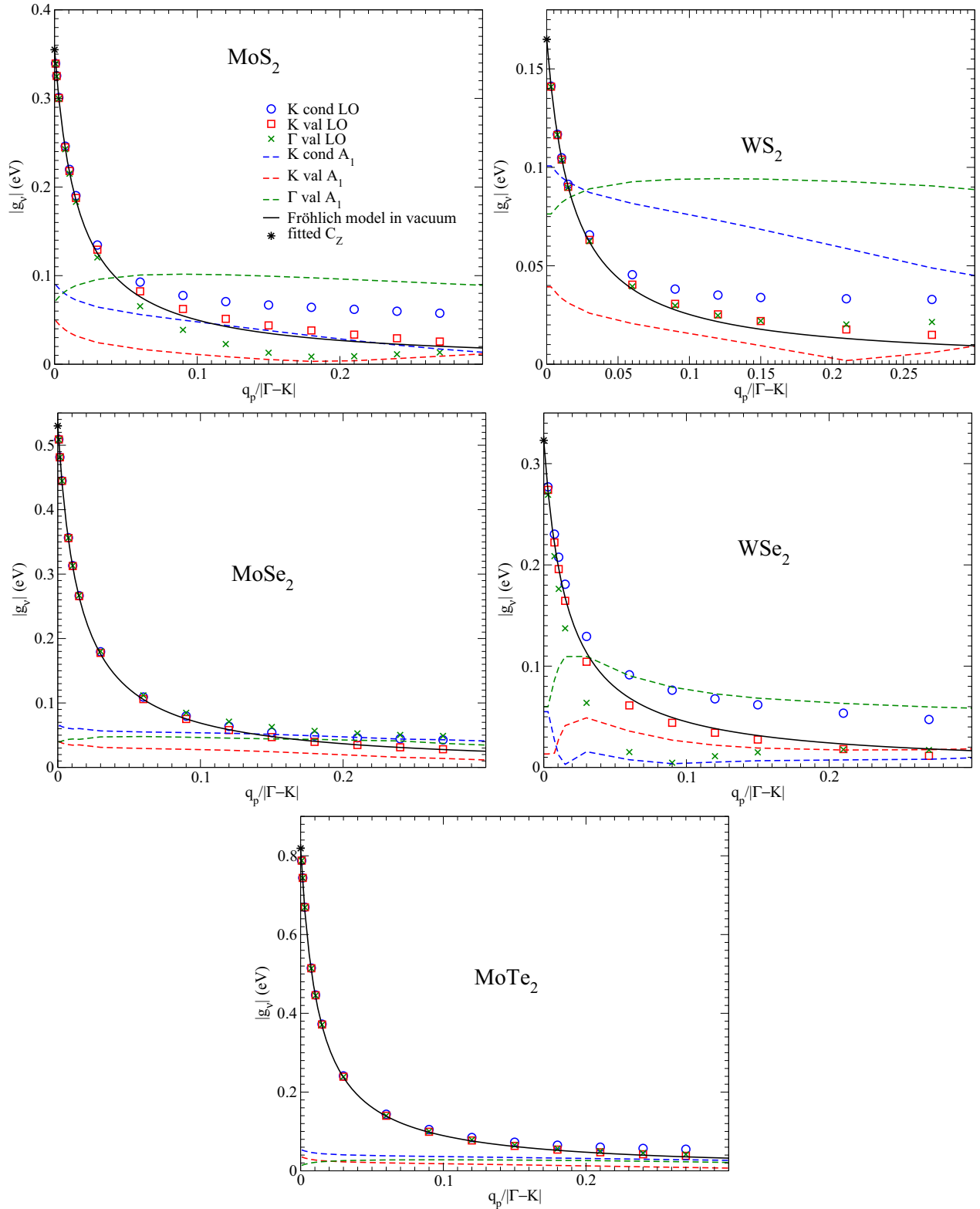$$+ (\epsilon_2 + \sqrt{\epsilon_p^m \epsilon_z^m}) c_2 e^{|\tilde{\mathbf{q}}_p| t/2}. \quad \text{(A17)}$$

FIG. 8. EPC matrix elements involving LO and A_1 phonon modes in monolayer MoS_2, $MoSe_2$, $MoTe_2$, WS_2, and WSe_2. We consider intraband scattering of electrons or holes in the conduction band near **K** ("K cond") and in the valence band near **K** and Γ ("K val" and "Γ val," respectively). Momenta $\mathbf{q}_p$ are in the $\Gamma \to \mathbf{M}$ direction. The analytical model of the Fröhlich interaction in its simplest isotropic form and using the parameters indicated in Table IV is shown in black solid lines. Dashed lines and symbols are DFPT calculations.

By defining the dielectric mismatches

$$\alpha_1 = \frac{\epsilon_z^m - \epsilon_1}{\sqrt{\epsilon_p^m \epsilon_z^m} + \epsilon_1}, \quad \bar{\alpha}_2 = \frac{\sqrt{\epsilon_p^m \epsilon_z^m} - \epsilon_2}{\sqrt{\epsilon_p^m \epsilon_z^m} + \epsilon_2},$$

$$\alpha_2 = \frac{\epsilon_z^m - \epsilon_2}{\sqrt{\epsilon_p^m \epsilon_z^m} + \epsilon_2}, \quad \bar{\alpha}_1 = \frac{\sqrt{\epsilon_p^m \epsilon_z^m} - \epsilon_1}{\sqrt{\epsilon_p^m \epsilon_z^m} + \epsilon_1}, \quad \text{(A18)}$$

we finally have

$$c_1 = \frac{C_{\mathcal{Z}}}{\sqrt{\epsilon_p^m \epsilon_z^m}} \frac{1 - e^{-|\tilde{\mathbf{q}}_p|t}}{|\mathbf{q}_p|t} \frac{\alpha_1 + \bar{\alpha}_1 \alpha_2 e^{-|\tilde{\mathbf{q}}_p|t}}{1 - \bar{\alpha}_1 \bar{\alpha}_2 e^{-2|\tilde{\mathbf{q}}_p|t}} e^{-|\tilde{\mathbf{q}}_p|t/2}, \quad \text{(A19)}$$

$$c_2 = \frac{C_{\mathcal{Z}}}{\sqrt{\epsilon_p^m \epsilon_z^m}} \frac{1 - e^{-|\tilde{\mathbf{q}}_p|t}}{|\mathbf{q}_p|t} \frac{\alpha_2 + \bar{\alpha}_2 \alpha_1 e^{-|\tilde{\mathbf{q}}_p|t}}{1 - \bar{\alpha}_1 \bar{\alpha}_2 e^{-2|\tilde{\mathbf{q}}_p|t}} e^{-|\tilde{\mathbf{q}}_p|t/2}. \quad \text{(A20)}$$

The Fröhlich interaction is thus

$$g_{\mathrm{Fr}}^{\mathrm{2D}}(\mathbf{q}_p) = \frac{1}{t} \int_{-t/2}^{t/2} [V_p(\mathbf{q}_p,z) + V_h(\mathbf{q}_p,z)] dz \quad \text{(A21)}$$

$$g_{\mathrm{Fr}}^{\mathrm{2D}}(\mathbf{q}_p) = \frac{C_{\mathcal{Z}}}{\sqrt{\epsilon_p^m \epsilon_z^m}} \left[\frac{2}{|\tilde{\mathbf{q}}_p|t} \left(1 + \frac{e^{-|\tilde{\mathbf{q}}_p|t} - 1}{|\tilde{\mathbf{q}}_p|t} \right) + \frac{(1 - e^{-|\tilde{\mathbf{q}}_p|t})^2}{|\mathbf{q}_p|t |\tilde{\mathbf{q}}_p|t} \frac{\alpha_1 + \alpha_2 + (\bar{\alpha}_1 \alpha_2 + \bar{\alpha}_2 \alpha_1) e^{-|\tilde{\mathbf{q}}_p|t}}{1 - \bar{\alpha}_1 \bar{\alpha}_2 e^{-2|\tilde{\mathbf{q}}_p|t}} \right]. \quad \text{(A22)}$$

The isotropic solution is ($\epsilon_p^m = \epsilon_z^m = \epsilon_{\mathrm{iso}}^m$)

$$g_{\mathrm{Fr}}^{\mathrm{2D}}(\mathbf{q}_p) = \frac{C_{\mathcal{Z}}}{\epsilon_{\mathrm{iso}}^m} \left[\frac{2}{|\mathbf{q}_p|t} \left(1 + \frac{e^{-|\mathbf{q}_p|t} - 1}{|\mathbf{q}_p|t} \right) + \frac{(1 - e^{-|\mathbf{q}_p|t})^2}{(|\mathbf{q}_p|t)^2} \frac{\alpha_1 + \alpha_2 + 2\alpha_1 \alpha_2 e^{-|\mathbf{q}_p|t}}{1 - \alpha_1 \alpha_2 e^{-2|\mathbf{q}_p|t}} \right]. \quad \text{(A23)}$$

APPENDIX B: COUPLING WITH OPTICAL PHONONS IN TMDs

In Fig. 8 we plot the small-momentum coupling to the A_1 and LO modes in monolayer TMDs MoS$_2$, MoSe$_2$, MoTe$_2$, WS$_2$, and WSe$_2$. Note that that WSe$_2$ is similar to MoS$_2$. WS$_2$ shows significantly smaller Fröhlich interaction. MoSe$_2$ and MoTe$_2$ are similar to each other, with large Fröhlich interaction and some different trends in the A_1 mode. Note also that the analytical model coincides relatively well with the DFPT results for the valence band at **K** in every material.

[1] B. Radisavljevic, A. Radenovic, J. Brivio, V. Giacometti, and A. Kis, Single-layer MoS$_2$ transistors, Nat. Nanotechnol. **6**, 147 (2011).

[2] Q. H. Wang, K. Kalantar-Zadeh, A. Kis, J. N. Coleman, and M. S. Strano, Electronics and optoelectronics of two-dimensional transition metal dichalcogenides, Nat. Nanotechnol. **7**, 699 (2012).

[3] D. Jariwala, V. K. Sangwan, L. J. Lauhon, T. J. Marks, and M. C. Hersam, Emerging device applications for semiconducting two-dimensional transition metal dichalcogenides, ACS Nano **8**, 1102 (2014).

[4] R. Ganatra and Q. Zhang, Few-layer MoS$_2$: A promising layered semiconductor, ACS Nano **8**, 4074 (2014).

[5] G. Fiori, F. Bonaccorso, G. Iannaccone, T. Palacios, D. Neumaier, A. Seabaugh, S. K. Banerjee, and L. Colombo, Electronics based on two-dimensional materials, Nat. Nanotechnol. **9**, 768 (2014).

[6] G. Moody, C. K. Dass, K. Hao, C.-H. Chen, L.-J. Li, A. Singh, K. Tran, G. Clark, X. Xu, G. Berghäuser, E. Malic, A. Knorr, and X. Li, Intrinsic homogeneous linewidth and broadening mechanisms of excitons in monolayer transition metal dichalcogenides, Nat. Commun. **6**, 8315 (2015).

[7] H. Wang, C. Zhang, and F. Rana, Ultrafast dynamics of defect-assisted electron-hole recombination in monolayer MoS$_2$, Nano Lett. **15**, 339 (2015).

[8] H. Shi, R. Yan, S. Bertolazzi, J. Brivio, B. Gao, A. Kis, D. Jena, H. G. Xing, and L. Huang, Exciton dynamics in suspended monolayer and few-layer MoS$_2$ 2D crystals, ACS Nano **7**, 1072 (2013).

[9] S. Baroni, S. De Gironcoli, A. Dal Corso, and P. Giannozzi, Phonons and related crystal properties from density-functional perturbation theory, Rev. Mod. Phys. **73**, 515 (2001).

[10] P. Vogl, Microscopic theory of electron-phonon interaction in insulators or semiconductors, Phys. Rev. B **13**, 694 (1976).

[11] S. D. Sarma and B. A. Mason, Optical phonon interaction effects in layered semiconductor structures, Ann. Phys. **163**, 78 (1985).

[12] N. Mori and T. Ando, Electronoptical-phonon interaction in single and double heterostructures, Phys. Rev. B **40**, 6175 (1989).

[13] J. Sjakste, N. Vast, M. Calandra, and F. Mauri, Wannier interpolation of the electron-phonon matrix elements in polar semiconductors: Polar-optical coupling in GaAs, Phys. Rev. B **92**, 054307 (2015).

[14] T. Sohier, M. Calandra, and F. Mauri, Density-functional calculation of static screening in two-dimensional materials: The long-wavelength dielectric function of graphene, Phys. Rev. B **91**, 165428 (2015).

[15] L. V. Keldysh, Coulomb interaction in thin semiconductor and semimetal films, Zh. Eksp. Teor. Fiz. Pis. Red. **29**, 716 (1979) [JETP Lett. **29**, 658 (1979)].

[16] P. Cudazzo, I. V. Tokatly, and A. Rubio, Dielectric screening in two-dimensional insulators: Implications for excitonic and impurity states in graphane, Phys. Rev. B **84**, 085406 (2011).

[17] T. O. Wehling, E. Sasioglu, C. Friedrich, A. I. Lichtenstein, M. I. Katsnelson, and S. Blügel, Strength of Effective Coulomb Interactions in Graphene and Graphite, Phys. Rev. Lett. **106**, 236805 (2011).

[18] T. C. Berkelbach, M. S. Hybertsen, and D. R. Reichman, Theory of neutral and charged excitons in monolayer transition metal dichalcogenides, Phys. Rev. B **88**, 045318 (2013).

[19] A. Steinhoff, M. Rösner, F. Jahnke, T. O. Wehling, and C. Gies, Influence of excited carriers on the optical and electronic properties of MoS_2, Nano Lett. **14**, 3743 (2014).

[20] K. Kaasbjerg, K. S. Thygesen, and K. W. Jacobsen, Phonon-limited mobility in n-type single-layer MoS_2 from first principles, Phys. Rev. B **85**, 115317 (2012).

[21] X. Li, J. T. Mullen, Z. Jin, K. M. Borysenko, M. B. Nardelli, and K. W. Kim, Intrinsic electrical transport properties of monolayer silicene and MoS_2 from first principles, Phys. Rev. B **87**, 115418 (2013).

[22] Z. Jin, X. Li, J. T. Mullen, and K. W. Kim, Intrinsic transport properties of electrons and holes in monolayer transition-metal dichalcogenides, Phys. Rev. B **90**, 045422 (2014).

[23] M. Danovich, I. Aleiner, N. D. Drummond, and V. Fal'ko, Fast relaxation of photo-excited carriers in 2D transition metal dichalcogenides, arXiv:1510.06288.

[24] T. Sohier, *Electrons and phonons in graphene: Electron-phonon coupling, screening and transport in the field effect setup*, Ph.D. thesis, Universite Pierre et Marie Curie, Paris VI, 2015.

[25] P. Giannozzi *et al.*, QUANTUM ESPRESSO: A modular and open-source software project for quantum simulations of materials, J. Phys.: Condens. Matter **21**, 395502 (2009).

[26] I. E. Castelli *et al.*, see http://www.materialscloud.org/sssp.

[27] N. V. Podberezskaya, S. A. Magarill, N. V. Pervukhina, and S. V. Borisov, Crystal chemistry of dichalcogenides MX_2, J. Struc. Chem. **42**, 654 (2001).

[28] T. Brumme, M. Calandra, and F. Mauri, First-principles theory of field-effect doping in transition-metal dichalcogenides: Structural properties, electronic structure, Hall coefficient, and electrical conductivity, Phys. Rev. B **91**, 155436 (2015).

[29] A. Molina-Sánchez and L. Wirtz, Phonons in single-layer and few-layer MoS_2 and WS_2, Phys. Rev. B **84**, 155413 (2011).

[30] J. Tóbik and A. Dal Corso, Electric fields with ultrasoft pseudo-potentials: Applications to benzene and anthracene, J. Chem. Phys. **120**, 9934 (2004).

[31] E. K. Yu, D. A. Stewart, and S. Tiwari, *Ab initio* study of polarizability and induced charge densities in multilayer graphene films, Phys. Rev. B **77**, 195406 (2008).

[32] C. Freysoldt, P. Eggert, P. Rinke, A. Schindlmayr, and M. Scheffler, Screening in two dimensions: GW calculations for surfaces and thin films using the repeated-slab approach, Phys. Rev. B **77**, 235428 (2008).

[33] D. Jena and A. Konar, Enhancement of Carrier Mobility in Semiconductor Nanostructures by Dielectric Engineering, Phys. Rev. Lett. **98**, 136805 (2007).

[34] A. Kormányos, G. Burkard, M. Gmitra, J. Fabian, V. Zólyomi, N. D. Drummond, and V. Fal'ko, $\mathbf{k} \cdot \mathbf{p}$ theory for two-dimensional transition metal dichalcogenide semiconductors, 2D Mater. **2**, 022001 (2015).